ELSEVIER

Journal of Crystal Growth 179 (1997) 618–624

JOURNAL OF CRYSTAL GROWTH

Kinetics and mechanism of methane hydrate formation and decomposition in liquid water Description of hysteresis

Knut Lekvam[a], Peter Ruoff[b,*]

[a] *RF-Rogaland Research, P.O. Box 2503, Ullandhaug, 4004 Stavanger, Norway*
[b] *School of Technology and Science, Stavanger College, P.O. Box 2557, Ullandhaug, 4004 Stavanger, Norway*

Received 15 February 1997

Abstract

Hysteresis in the formation and decomposition (melting) of methane hydrate as a function of temperature has been studied. Here we show how hysteresis can be modelled by a set of pseudo-elementary processes. The model is based on a previously proposed reaction scheme for the formation of methane hydrate in liquid water. The simulation calculations agree quantitatively with the shapes of experimental hysteresis curves. The model contains the first set of pseudo-elementary processes that successfully simulate the presence of an induction period, its subsequent reactive phase and the thermodynamic border between reactive and nonreactive methane/water mixtures.

1. Introduction

A variety of small-sized molecules, among them the components of natural gas, form with water, solid, crystalline clathrate compounds, so-called hydrates at low temperature and high pressure [1–7]. Although hydrates are known since the beginning of the 19th century [8], it was the discovery of natural gas hydrates as plugs in pipelines that initiated first systematic studies [9–12].

Investigations on the kinetics of gas hydrate growth started in the beginning of the 1960s. Hydrate formation in systems with solid ice [13–18] and liquid water [3, 19–25] have been investigated. Empirical models that describe the macroscopic growth of hydrate were developed [15–18, 22–26].

Regarding the kinetics of dissociation of hydrates, primary focus has been on the decomposition of hydrates in porous media. With one exception [27], the kinetics of hydrate dissociation in porous media, have been treated as pure mass- and heat-transfer problems. Only few models [15, 28–30] are dealing with the intrinsic rate of dissociation of the hydrates.

Experimentally, very often, induction periods are observed, i.e., a certain time is required from the moment the reagents are mixed until the hydrate is

* Corresponding author. Fax: + 47 518 31750.

PII S0022-0248(97)00166-8

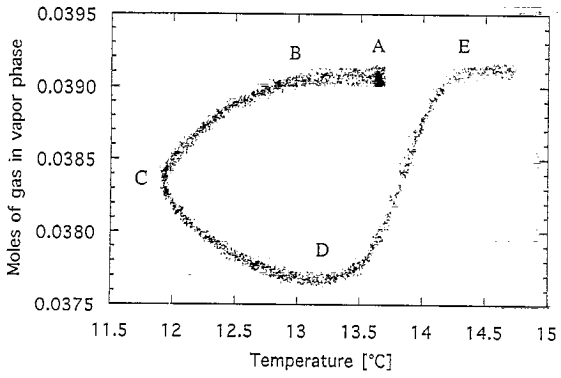

Fig. 1. Experimentally obtained hysteresis in the formation and melting of methane hydrate. The number of moles in the 14 ml large gas phase calculated from the measured pressure during 8 repetitive cycles are plotted vs. temperature. The cooling and heating gradient was ± 3.0 K h^{-1}. (A) The system is equilibrated for 1 h and the cycle starts by cooling the system from 13.8°C. (B) The first appearance of hydrates. (C) Heating of the system starts. (D) The hydrate equilibrium line is crossed and hydrate begins to melt. (E) The last visual hydrate particles have disappeared from the solution.

formed. Depending on the nature of the guest molecules [13, 14, 16] and whether water was in contact previously with hydrate [3, 22, 31], induction period lengths were found to vary considerably and in an apparently random fashion.

When phase diagrams of gas hydrates are experimentally determined, the temperature is periodically cycled between a maximum and a minimum value. It is under these conditions when hysteresis is observed. A typical example of hysteresis in one of our methane hydrate systems is shown in Fig. 1.

On the basis of experimental studies, we recently described a reaction kinetic model [32, 33] for the formation of methane hydrate in liquid water. Experimental hysteresis would provide an additional test about the applicability and generality of this model. In this paper, we show that some slight adjustments have to be made in order to model quantitatively hysteresis in the methane hydrate–liquid water system.

2. Experimental results

The experimental setup, conditions, and purities of chemicals in this work have been the same as described previously [32, 33]. In the experiments, methane and water were kept in a closed reactor with constant stirring rate at 980 rpm. The whole reactor was immersed into a water bath whose temperature could decrease or increase in time at a constant rate. Gas and water temperatures inside the reactor, as well as temperature of the water bath were monitored simultaneously.

After a variety of initial experiments, it was chosen to conduct the experiments only with cooling/heating rates that were lower than 3 K h^{-1}. The reason for this was that for such low-temperature changes the formed hydrate appears evenly dispersed in the water phase. When higher cooling rates were used, the hydrate was formed in larger aggregates that caused distortions in the hysteresis curve, especially at rising temperatures when the large hydrate particles started to melt.

For each cooling/heating rate a series of 7 or more parallel runs (cycles) were recorded. Fig. 1 shows the reproducibility of 8 repetitive 3 K h^{-1} cycles. Before a cycle was started, methane hydrate was prepared inside the reactor. The hydrate was then melted by keeping the temperature at 13.8°C for 2 h, then cooling of the reactor was started.

The shape of the hysteresis curve is affected by the cooling rate. Fig. 2 shows the hysteresis for 3 different cooling/heating rates. Before the hydrate started to melt, the hydrate crystals were partly transparent. However, during the melting process of the hydrate (at the temperature-rising branch of the hysteresis curve) it was observed that the bulk containing both water and hydrate turned opaque. We explain the opaqueness due to the appearance of tiny gas bubbles on the surface of the hydrate crystals.

2.1. The model

A previously proposed model for the formation of methane hydrate in liquid water [32] is used as a basis for this study. The model was originally designed to account for the presence of an induction period and for the sudden appearance of hydrate at the end of the induction period. It consists of the following five pseudo-elementary

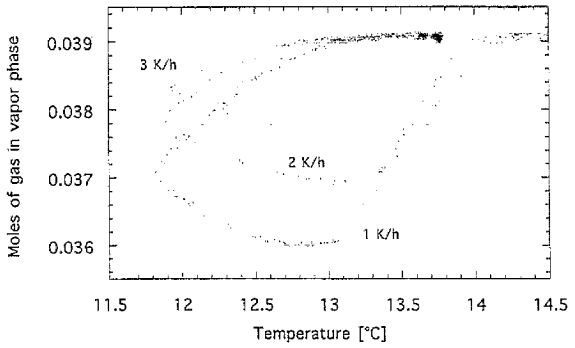

Fig. 2. Experimentally obtained hydrate formation cycles with different cooling and heating gradients. The number of moles in the 14 ml large gas phase calculated from the measured pressure during a temperature cycle are plotted vs. the temperature. Temperature gradients have been ± 3, ± 2 and $\pm 1\ K\ h^{-1}$.

processes:

$$CH_4\ (g) \underset{k_{-1}}{\overset{k_1}{\rightleftharpoons}} CH_4\ (aq), \tag{M1}$$

$$f CH_4\ (aq) + hH_2O \underset{k_{-2}}{\overset{k_2}{\rightleftharpoons}} N, \tag{M2}$$

$$N \overset{k_3}{\rightarrow} H, \tag{M3}$$

$$N \underset{k_{-4}}{\overset{k_4[H]}{\rightleftharpoons}} H, \tag{M4}$$

$$f CH_4\ (aq) + hH_2O \underset{k_{-5}}{\overset{k_5[H]}{\rightleftharpoons}} H. \tag{M5}$$

Process (M1) describes the dissolution of methane into the water phase. Reaction (M2) describes the formation of an oligomeric intermediate, N, while process (M3) is a slow (uncatalyzed) formation of macroscopic methane hydrate crystals H from N. The macroscopic growth of methane hydrate crystals occurs due to the autocatalytic processes (M4) and (M5). While (M4) describes the growth of methane hydrate crystals from precursor N, process (M5) represents the formation of methane hydrate directly from the reaction between water and the dissolved gas.

2.1.1. Bubble formation during hydrate melting

A factor that was not incorporated in our model [32, 33] was the appearance of bubbles during the melting of hydrate. Initial simulations with our previous model [32, 33] showed that under melting conditions the experimental pressure was building up much more rapidly than the calculations suggested. We therefore saw it necessary to incorporate bubble formation into our model.

Generally, bubbles may nucleate in two ways: homogeneously or/and heterogeneously. Homogeneous nucleation occurs spontaneously when the supersaturation reaches a limit; the spinodal point. Below this limit, induction times are observed, showing inverse proportionality with the level of supersaturation. Heterogeneous nucleation occurs when nucleation is initiated by certain inhomogeneities in the solution (seeds). Heterogeneous nucleation occurs usually at much lower supersaturation values.

During the melting process, the bulk phase is filled with hydrate crystals which make suitable growth sites for bubbles. We therefore believe that the nucleation of bubbles during melting is strongly heterogeneous. It appears difficult to predict at which supersaturation nucleation will occur, but it is probably much lower than the spinodal point. For the sake of simplicity, we assume that the critical saturation value is of the same order of magnitude as the two-phase liquid–vapor equilibrium. At this limit, the gas escaping from the solution by bubbles behaves like a step function [34]. When the dissolved methane concentration falls below this limit, nucleation terminates again. The application of step functions to describe the nucleation of bubbles has previously been used successfully in the modelling of homogeneous nucleation of bubbles in gas evolution oscillators [34–36].

In the model we incorporate the formation of bubbles during melting as the following irreversible reaction:

$$CH_4\ (aq) \overset{k_6}{\rightarrow} CH_4\ (g). \tag{M6}$$

Because bubble formation is only involved when a certain supersaturation of dissolved gas is present, this step will not affect the equilibrium of the system.

2.1.2. Constraints on rate constants

In a closed system, as studied experimentally here, any reaction will finally reach equilibrium. According to the principle of detailed balance [37] each of the component processes (M1)–(M5) will therefore attain equilibrium, which leads to the following expressions:

$$\frac{[CH_4\ (aq)]}{[CH_4\ (g)]} = \frac{k_1}{k_{-1}}, \tag{E1}$$

$$\frac{N}{[CH_4\ (aq)]^f [H_2O]^h} = \frac{k_2}{k_{-2}}, \tag{E2}$$

$$N = \frac{k_{-4}[H]}{k_3 + k_4[H]}, \tag{E3}$$

$$[CH_4\ (aq)]^f [H_2O]^h = \frac{k_{-5}}{k_5}. \tag{E4}$$

Because at equilibrium $k_3 \ll k_4[H]$ [32, 33], Eq. (E3) takes the form

$$N = \frac{k_{-4}}{k_4}. \tag{E3'}$$

Combination of Eqs. (E2), (E3) and (E4) results in the following relationship between rate constants $k_{\pm i}$ for $i = 2$, 4 and 5:

$$\frac{k_2}{k_{-2}} \frac{k_{-5}}{k_5} = \frac{k_{-4}}{k_4}. \tag{1}$$

The k_1/k_{-1} ratio can be determined experimentally [32, 33].

The influence of temperature T on rate constant k_i is assumed to be described by a simple Arrhenius relationship

$$k_i = A_i \exp\left(-\frac{E_i}{RT}\right), \tag{2}$$

where A_i and E_i are temperature-independent constants. E_i is the activation energy. Experimentally, the equilibrium concentration of dissolved methane has been determined as a function of temperature. Fig. 3 shows $[CH_4\ (aq)]^f$ as a function of $1/T$, where f is the average stoichiometric coefficient [32] of processes (M2) and (M5).

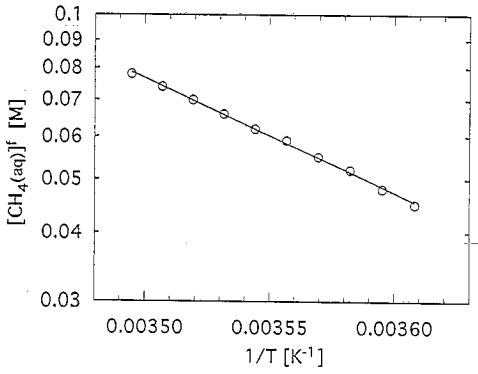

Fig. 3. Equilibrium phase diagram. Based on the measured equilibrium points for different pressures and temperatures, the equilibrium concentration of dissolved gas has been calculated and plotted in the power of the stoichiometric factor, f, vs. the reciprocal temperature.

From Eq. (E4) we write

$$\ln [CH_4\ (aq)]^f = \ln \frac{A_{-5}}{A_5} - \frac{1}{RT}(E_{-5} - E_5) \tag{3}$$

and according to Eq. (1)

$$\ln [CH_4\ (aq)]^f = \ln \frac{A_{-4}A_{-2}}{A_4A_2} - \frac{1}{RT}(E_{-4} + E_{-2} - E_4 - E_2). \tag{4}$$

From the experimentally determined slope in Fig. 3, we have the following constraints in activation energies:

$$E_{-5} - E_5 = E_{-2} + E_{-4} - (E_2 + E_4) = 4326\ \text{J/mol}. \tag{5}$$

These constraints from equilibrium considerations have to be taken into account when activation energies and rate constants are chosen in order to model experimental behavior.

3. Simulation results and discussion

Table 1 shows the rate constants, their activation energies and the nucleation threshold for bubble

Table 1
Rate constant values and activation energies

Rate constant[a]	Value (6°C)	Activation energy (kJ/mol)
k_1	$0.01341\ \mathrm{min}^{-1}$	0
k_{-1}	$0.449\ \mathrm{min}^{-1}$	12.4
k_2	$1.1\times10^{-13}\ \mathrm{M}^{1-f-h}\ \mathrm{min}^{-1}$	60
k_{-2}	$3.7\times10^{-2}\ \mathrm{min}^{-1}$	0
k_3	$3\times10^{-5}\ \mathrm{min}^{-1}$	0
k_4	$1.8\times10^{9}\ \mathrm{M}^{-1}\ \mathrm{min}^{-1}$	0
k_{-4}	$2.8\times10^{6}\ \mathrm{min}^{-1}$	96.0
k_5	$1.9\times10^{-3}\ \mathrm{M}^{-f-h}\ \mathrm{min}^{-1}$	0
k_{-5}	$1\times10^{6}\ \mathrm{min}^{-1}$	36.0
k_6	$\begin{cases}0, & \text{if } S\leqslant 1.02^{b}\\ 2.0\ \mathrm{min}^{-1}, & \text{if } S>1.02^{b}\end{cases}$	0

[a] The rate constants k_1 and k_{-1} are determined experimentally [32]. The other rate constants give the best fit to experimental data.
[b] S is the supersaturation ratio between dissolved methane concentration in the aqueous phase [CH_4 (aq)] and the corresponding value [CH_4 (aq)]^{eq} that is in equilibrium with methane in the gas phase, i.e., $S = [CH_4\ (aq)]/[CH_4\ (aq)]^{eq}$.

formation used in our calculations. Rate constants k_1 and k_{-1} are those earlier determined by experiments [32], while the remaining rate constant values were optimized to fit the experimental results of Fig. 2. Fig. 4 shows three different calculated hysteresis cycles which correspond to the experimental results of Fig. 2. The simulations are in good quantitative agreement with experiments.

There is considerable interest in predicting induction times. Skovborg [38] suggested to use the $\Delta\mu_{H_2O}$ as a driving force in the nucleation of hydrates. $\Delta\mu_{H_2O}$ is the chemical potential difference for the *component* H_2O, between the aqueous liquid and the solid hydrate phase. They found that the induction time increased exponentially with increasing $\Delta\mu_{H_2O}$. The results of Skovborg [38] are analogous with the results of Lingelem and Majeed [39], where the induction time was reported as exponential with respect to subcooling, ΔT. We have simulated the induction times as constant temperature experiments with our model for different constant temperatures and different initial amounts of gas. The simulations gave a linear plot

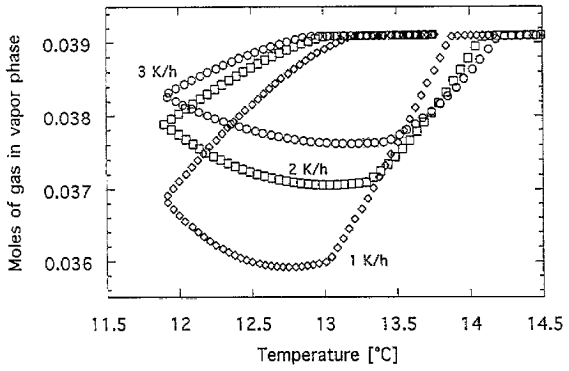

Fig. 4. Simulated hydrate formation cycles corresponding to the experiments of Fig. 2. The modelled number of moles in the 14 ml large gas phase during 3 temperature cycles are plotted vs. the temperature.

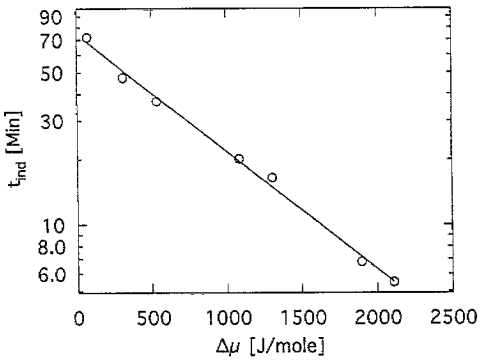

Fig. 5. Simulated induction times (logarithmic scale) versus calculated chemical potential difference, $\Delta\mu_{CH_4}$ between initial and equilibrium states. $\Delta\mu_{CH_4}$ is the chemical potential difference for the *component* CH_4, between the aqueous liquid and the solid hydrate phase. The relation is calculated from the chemical potential of gas prior to nucleation, and the chemical potential of gas at hydrate equilibrium.

for the induction times plotted as a function of $\Delta\mu_{CH_4}$ (Fig. 5). $\Delta\mu_{CH_4}$ is the chemical potential difference for the *component* CH_4, between the aqueous liquid and the solid hydrate phase. Natarajan et al. [40] have proposed a similar relationship as driving force. They use $(f_g/f_{eq} - 1)$, where f_g and f_{eq} are the fugacities of the initial and equilibrium state of the system. For small values, this relation is found to be a linearization [41] of the logarithmic expression, $\ln f_g/f_{eq}$, which is recognized as a part of Lewis' $\Delta\mu$ expression [42].

The kinetic scheme (M1)–(M6) represents the first set of pseudo-elementary processes that successfully simulate the presence of an induction period, its subsequent reactive phase [32, 33], and the thermodynamic border between reactive and non-reactive methane/water mixtures. The model's quantitative estimates concerning induction period length (Fig. 5), reaction rates of hydrate formation (Fig. 6 in Ref. [32]) and melting (Fig. 4) appear in good agreement with corresponding experiments.

With the ability to describe/simulate hysteresis the model is also able to predict the influence of kinetic parameters on thermodynamic properties of hydrate systems. As an example, it may be of interest to study the influence of individual rate constants on the border that separates the thermodynamic conditions, where methane hydrate may form or dissociate (Fig. 2 in Ref. [32]). This may be of importance to identify those kinetic steps that may help to obtain conditions for a "kinetic control" in the avoidance of gas hydrate formation [43].

One part of our model that probably will need further refinement is the size distribution of the oligomeric precursor N and the influence of these various precursor forms on the overall kinetics. Another part concerns the kinetics of bubble formation during melting, which so far are approximately described by the sudden onset of reaction (M6) as soon as the supersaturation threshold has been exceeded.

4. Conclusions

The experimentally obtained temperature hysteresis is quantitatively modelled by our earlier proposed model [32, 33] and autocatalysis appears to be an essential part of the hydrate formation process.

The model describes the kinetics as well as the thermodynamics of the liquid–solid phase transitions when applying temperature gradients.

There is a strong influence of bubble nucleation on transport of gas out of solution during hydrate dissociation. The mechanisms of hydrate decomposition might be more complex and should be investigated further.

Acknowledgements

K.L. thanks Esso Norge for financial support.

References

[1] W. Schroeder, in: Die Geschichte der Gashydrate, Sammlung Chemischer und Chemisch-Technischer Vorträge, vol. 29, Ferdinand Enke, Stuttgart, 1926.
[2] D.W. Davidson, Water in crystalline hydrates, aqueous solutions of simple nonelectrolytes, in: F. Franks (Ed.), Water – a comprehensive Treatise, vol. 2, Plenum, New York, 1973, ch. 3, pp. 115–234.
[3] Y.F. Makogon, Hydrates of Natural Gas, PennWell, Tulsa (Engl. Transl.) 1981, Gidraty prirodnykh gazov, M. Nedra, Moscow, 1974.
[4] J. Finjord, Hydrates of natural gas, a state-of-the-art study with emphasis on fundamental properties, Tech. Report No. T11/83, Rogaland Research Institute, Stavanger, 1983.
[5] E. Berecz, M. Balla-Achs, Gas Hydrates, Akadémiai Kiadó, Budapest, 1983.
[6] E.D.J. Sloan, Clathrate Hydrates of Natural Gases, Dekker, New York, 1990.
[7] P. Englezos, Ind. Eng. Chem. Res. 32 (1993) 1251.
[8] H. Davy, Philos. Trans. Ser. B 101 (1811) 1.
[9] E.G. Hammerschmidt, Ind. Eng. Chem. 26 (1934) 852.
[10] M. Stackelberg, Naturwissenschaften 36 (1949) 327.
[11] M. Stackelberg, Naturwissenschaften 36 (1949) 359.
[12] M. Stackelberg, H.R. Müller, Z. Electrochem. 58 (1954) 25.
[13] R.M. Barrer, D.J. Ruzicka, Trans. Faraday. Soc. 58 (1962) 2262.
[14] R.M. Barrer, V.J. Edge, Proc. Roy. Soc. (London) A 300 (1967) 1.
[15] S.L. Miller, W.D. Smythe, Science 170 (1970) 531.
[16] B.J. Falabella, PhD Thesis, University of Massachusetts, 1975.
[17] V.A. Kamath, PhD Thesis, University of Pittsburgh, 1984.
[18] M.J. Hwang, D.A. Wright, A. Kapur, G.D. Holder, J. Inclusion Phenomena Molecular Recognition Chem. 8 (1990) 103.
[19] W.G. Knox, M. Hess, G.E. Jones, H.B. Smith, Chem. Eng. Prog. 57 (2) (1961) 66.
[20] B.B. Maini, P.R. Bishnoi, Chem. Eng. Sci. 36 (1981) 183.
[21] D.R. Topham, Chem. Eng. Sci. 39 (1984) 821.
[22] A. Vysniauskas, P.R. Bishnoi, Chem. Eng. Sci. 38 (1983) 1061.
[23] A. Vysniauskas, P.R. Bishnoi, Chem. Eng. Sci. 40 (1985) 299.
[24] P. Englezos, N. Kalogerakis, P.D. Dholabhai, P.R. Bishnoi, Chem. Eng. Sci. 42 (1987) 2647.
[25] P. Englezos, N. Kalogerakis, P.D. Dholabhai, P.R. Bishnoi, Chem. Eng. Sci. 42 (1987) 2659.
[26] P. Skovborg, P. Rasmussen, Chem. Eng. Sci. 49 (1994) 1131.

[27] M.H. Yousif, H.H. Abass, M.S. Selim, E.D. Sloan, Presented at 63th Annu. Tech. Conf. Exhibit. of the Society of Petroleum Engineers, 2–5 October 1988, Houston, TX; Paper No. 18320, Society of Petroleum Engineers, Richardson, TX.
[28] H.C. Kim, P.R. Bishnoi, R.A. Heideman, S.S.H. Rizvi, Chem. Eng. Sci. 42 (1987) 1645.
[29] A.K.M. Jamaluddin, N. Kalogerakis, P.R. Bishnoi, Can. J. Chem. Eng. 67 (1989) 948.
[30] G.B. Guo, R.E. Bretz, R.L. Lee, in: Proc. 1992 Internat. Gas Res. Conf. 16–19 November 1992, Orlando, FL. 1992, pp. 231–240, Gas Research Institute, Chicago, IL, 1992.
[31] J.P. Schroeter, R. Kobayashi, H.A. Hildebrand, Hydrate decomposition conditions in the system hydrogen sulfide–methane, and propane, Tech. Pub. TP-10, 1983; Gas Processors Association, Tulsa, OK.
[32] K. Lekvam, P. Ruoff, J. Am. Chem. Soc. 115 (1993) 8565.
[33] K. Lekvam, P. Ruoff, J. Am. Chem. Soc. 116 (1994) 4529.
[34] S.M. Kaushik, R.M. Noyes, J. Phys. Chem. 89 (1985) 2027.
[35] M.B. Rubin, R.M. Noyes, J. Phys. Chem. 91 (1987) 4193.
[36] R.M. Noyes, M.B. Rubin, P.G. Bowers, J. Phys. Chem. 96 (1992) 1000.
[37] J.W. Moore, R.G. Pearson, Kinetics and Mechanism, 3rd ed., Wiley, New York, 1981, pp. 307–309.
[38] P. Skovborg, PhD Thesis, Danmarks Tekniske Højskole, Lyngby, Denmark, 1993.
[39] M. Lingelem, A. Majeed, in: Proc. 68th. Ann. Gas Proc. Assoc. Convention, San Antonio, TX, 13–14 March 1989; Gas Processors Association, Tulsa, OK, pp. 19–29.
[40] V. Natarajan, P.R. Bishnoi, N. Kalogerakis, Chem. Eng. Sci. 49 (1994) 2075.
[41] R.L. Christiansen, V. Bansal, E.D. Sloan, Presented at University of Tulsa Centennial Petroleum Engineering Symp., 29–31 August 1994, Tulsa, OK; Paper No. 27994, Society of Petroleum Engineers, Richardson, TX.
[42] J.M. Prausnitz, Molecular Thermodynamics of Fluid-Phase Equilibria, Prentice-Hall, Englewood Cliffs, NJ, 1969.
[43] M.A. Kelland, T.M. Svartaas, L.A. Dybvik, Presented at SPE 69th Annu. Tech. Conf. Exhibition, 25–28 September 1994, New Orleans, LA; Paper No. 28506, Society of Petroleum Engineers, Richardson, TX.